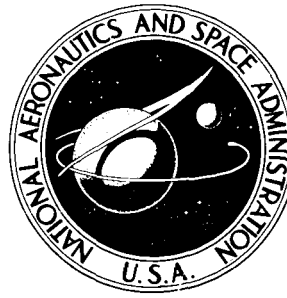


1969 003 1048

69N 40437

NASA TECHNICAL NOTE



NASA TN D-5522

NASA TN D-5522

**PENETRATION MODEL EXPLANATION
FOR TURBULENT FORCED-CONVECTION
HEAT TRANSFER OBSERVED IN
NEAR-CRITICAL FLUIDS**

by Robert W. Graham

Lewis Research Center

Cleveland, Ohio

PENETRATION MODEL EXPLANATION FOR TURBULENT FORCED-CONVECTION

HEAT TRANSFER OBSERVED IN NEAR-CRITICAL FLUIDS

by Robert W. Graham

Lewis Research Center

SUMMARY

The traditional steady-state model of turbulent convection in a thermal boundary layer has been modified to include a nonsteady penetration component of heat transfer. The penetration mechanism is assumed to result from appreciable changes in the specific volume of local agglomerates of fluid near the wall under heating conditions. In some respects the penetration mechanism is similar to boiling. The overall model has been applied to forced convection of several fluids near their critical thermodynamic state. Some success has been achieved in using the model to account for the differences between the experimental data and conventional turbulent flow heat-transfer correlations for variable property fluids.

INTRODUCTION

The peculiar forced-convection heat transfer by a fluid when it is near its thermodynamic critical point has been observed by numerous researchers (refs. 1 to 9). Needless to say, an explanation for these peculiar characteristics of heat transfer has been of considerable interest to the heat-transfer community.

For the most part, explanations of this behavior have centered on the unusual physical and transport properties of near-critical fluids. Efforts to correlate these data have involved manipulation of the fluid and transport properties as they are inserted into standard forced-convection correlations. In some cases, such as references 10 to 13, more elaborate analytical techniques were tried where variable property boundary layer analyses were applied. Such differential descriptions of the boundary layer, as contained in reference 10 or 14, were utilized.

While limited success has been realized in correlating some near-critical fluid heat-transfer data by the selection of reference fluid and transport properties, general success

by this method cannot be claimed. Consequently, other approaches need examination in rendering an explanation for the heat-transfer rates.

One obviously different approach is to attribute the heat-transfer behavior to a change in the turbulent mechanism. In 1954, Goldmann suggested that a boiling-like mechanism of the near-critical fluid may explain the heat transport. Some visual studies described in references 15 to 17 have lent credance to such an explanation. The boiling-like explanation was extended further by Hsu in his written comments to reference 6.

In 1966, Hall, Jackson, and Khan (ref. 18) suggested that the turbulent diffusion in the boundary layer may be amplified by the expansive coefficient of the fluid. They argued that they could relate their carbon dioxide heat-transfer data to such a mechanism and not to the near-critical values of the transport properties.

Herein, a somewhat different explanation which is based on a penetration model of the boundary layer is proffered. Hanratty (ref. 19) first suggested that the turbulent boundary layer could be represented by a penetration model. In the conventional turbulent heat-transfer approaches, the fluctuating components of velocity and temperature are represented by some statistical time-averaged value. Through averaging, one can eliminate time as a variable. In the penetration model approach, however, the time dependence is emphasized. The heat transfer is treated as a transient conduction process, which is repetitive as fluid species contact the wall. As is well known, the penetration model had its origin in gas-liquid diffusion processes and has been widely used in computations of processes in fluidized and liquid beds. Its more recent application to the turbulent boundary layer has been justified by evidence of turbulent-like behavior in the so-called laminar sublayer. Many references, such as 20 to 24, contain evidence of this sublayer turbulence which has been labeled by some as a "sublayer instability."

The heat-transfer model incorporating a penetration component is compared to the liquid hydrogen experimental data found in reference 25. These near-critical data have not been adequately correlated by standard correlation schemes. However, the relative success in correlating these data is used as a supporting argument for the introduction of a new mechanistic effect. The correlation equation developed for the hydrogen data is applied to a limited amount of heat-transfer data for near-critical carbon dioxide and water. The main purpose of this report is to present a proposal which takes into account the peculiar turbulent behavior of near-critical fluids.

SYMBOLS

- A area
- a frequency enhancement factor
- C constant

c	specific heat
D	diameter of channel
d	diameter of jet (appendix B)
G	mass flow per unit area
g	gravity
H	enthalpy
h	heat-transfer coefficient
J	mechanical equivalent of heat
k	thermal conductivity
L	length
Nu	Nusselt number
n	exponent
Q	heat rate
q	heat flux
Re	Reynolds number
St	Stanton number
T	temperature
U	velocity component, axial
V	velocity component, normal
v	specific volume
x	axial distance and quality fraction
y	normal distance
ρ	density
ω	frequency
μ	viscosity
φ	thermal boundary layer thickness
τ	time

Subscripts:

av	average
b	bulk

c	contact
enh	enhanced
exp	experimental
f	film
fg	film reference based on gas
fm	film reference based on two-phase mixture
i	wall temperature, inside pipe (eq. (6))
o	reference, adiabatic
p	penetration model
t	total

PROPOSED HEAT-TRANSFER MODEL

In view of the enhanced heat-transfer rate observed with near-critical fluids (as compared to a film correlation), it is proposed that this enhancement be represented by an additive term to the conventional film property forced-convection coefficient. In general, the average heat-transfer coefficient can be written as

$$h_{av} = C_1 h_f + C_2 h_{enh} \quad (1)$$

One can introduce an enhanced coefficient and the appropriate weighting coefficients C_1 and C_2 to enable correlation of the experimental data.

In this report it is proposed that the enhancement mechanism is "penetration." It is analogous to the penetration mechanism of packed beds in chemical engineering technology. The extreme density gradient through the boundary layer produces instabilities which disrupt the viscous, near-wall portion of the turbulent boundary layer. The penetration of this near-wall sublayer by fluid packets from the outer region of the boundary layer is the reason for the name of the mechanism. The weighting coefficients reflect area fractions of the surface where the penetration mechanism does and does not dominate.

A gross overall view of the penetration model and the involvement of an area-weighting factor is shown in figure 1. Equation (1) can be written particularly for the penetration enhancement model as follows:

$$h_{av} = \frac{A_p}{A_t} h_p + \left(1 - \frac{A_p}{A_t}\right) h_f \quad (2)$$

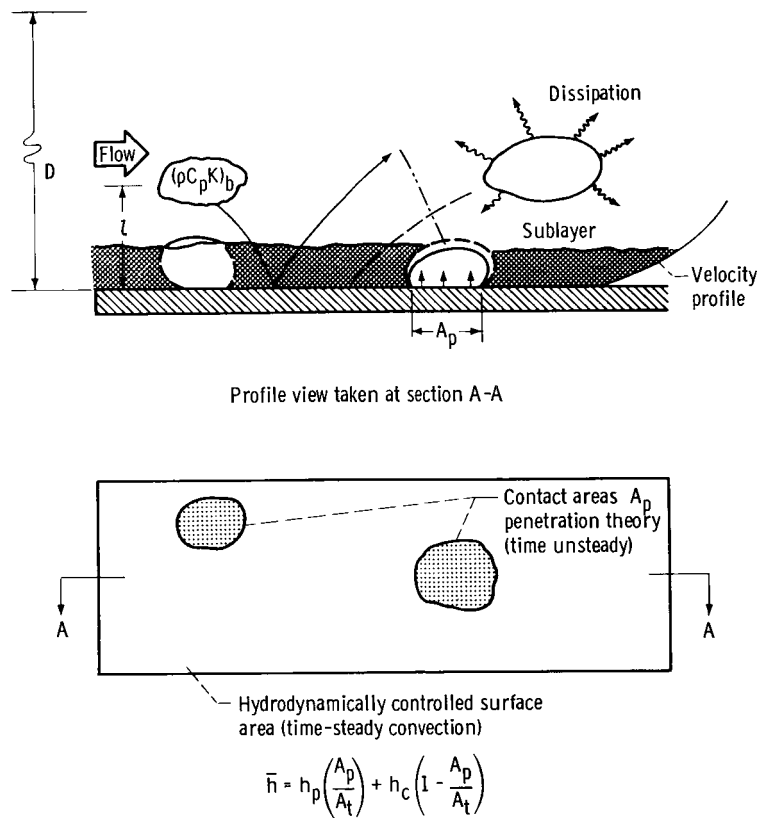


Figure 1. - Concept of simultaneous hydrodynamic and penetration mechanisms.

where

A_p/A_t penetration area fraction

h_p penetration coefficient

h_f conventional forced convection coefficient, evaluated at film properties

In this approach, the area fraction parameter and the penetration heat-transfer coefficient are only correlation parameters. The magnitude of these coefficients was established by the use of a limited amount of near-critical hydrogen data from references 25 and 26. Data points from 11 runs were used in determining the constants. The correlation method was eventually applied to a total of 50 hydrogen data runs; data from several axial stations were incorporated for each run. The run numbers for the 11 runs used in determining the constants are marked with an asterisk in tables I and II. The details of how the coefficients were estimated appears in appendix A.

In the prediction of the penetration heat-transfer coefficient, the essential elements are the bulk properties of the fluid and the frequency with which the packets disrupt the sublayer. The form of the equation is exactly similar to the one used to describe penetration heat-transfer coefficients in packed beds (ref. 30):

$$h_p = \frac{2}{\sqrt{\pi}} \sqrt{\omega (\rho c_p k)_b} \quad (3)$$

where ω is the frequency and the subscript b denotes bulk conditions.

As described in appendix A, the frequency is presumed dependent on density change in the boundary layer and on the average momentum of the axial flow in the boundary layer. The interaction of density change and flow momentum is considered in an analogous fashion to forced convection boiling. The behavior of the frequency term was computed from

$$\omega = \omega_0 \left[\frac{(\rho_b - \rho_w) \sqrt{2Jg_c(H_w - H_b)}}{\rho_f U_\infty} \frac{\mu_f}{\mu_b} \right] \quad (4)$$

The term in brackets, involving the density change, axial momentum of the boundary layer, etc., may be interpreted to be a dimensionless frequency enhancement factor. The term ω_0 in equation (4) is strictly an empirical frequency but it does turn out that its magnitude (20 cps) is within the range of frequency measurements made in the sublayer under adiabatic conditions. The enhancement factor is always much greater than one, so the frequency computed from equation (4) always exceeds the reference value ω_0 . Equation (4) is only applicable to the heating case where $\rho_b > \rho_w$.

Hydrodynamic arguments about mass transfer have served to rationalize the correlation form for the penetration area fraction used in estimating the average heat-transfer coefficient. The penetration area fraction weighting term is primarily a function of the heat-transfer rate. The rate can be represented by the bulk Stanton number. The correlating equation for the penetration area fraction is

$$\frac{A_p}{A_t} = C(St)_b^{0.8} \left(\frac{L}{D}\right)^{0.8} \quad (5)$$

This correlation scheme (described in greater detail in appendix A) was applied to the near-critical heat-transfer data for liquid hydrogen found in reference 25. As mentioned previously, 11 runs from reference 25 were utilized in determining the coefficients em-

pirically. Then, the correlation method was extended to most of the near-critical hydrogen heat-transfer data found in reference 25. It is important to observe that an upper limit to the magnitude of A_p/A_t was assigned. The value was approximately 0.16 and it is akin to the maximum area fraction observed on boiling surfaces near burnout conditions.

COMPARISON OF MODEL WITH EXPERIMENTAL DATA

Hydrogen

The mechanistic model of turbulent heat transfer as set forth in the previous section and appendix A was compared with experimental near-critical data for hydrogen, carbon dioxide, and water. The hydrogen data from reference 25 were the chief source of data. The empirical constants in the model were obtained from comparisons with selected near-critical hydrogen heat-transfer data from reference 25.

It was stated in the INTRODUCTION that the near-critical forced-convection data for hydrogen could not be correlated by a standard turbulent correlation. As an example of the disparity between a standard correlation and experimental data, the heat-transfer coefficient distributions along the axis of a tube are shown in figure 2. The range of L/D spans from 13 to 34. The circled points are experimental data, and the squares are predicted values from a turbulent pipe flow heat-transfer correlation. Note the wide discrepancy between prediction and experiment for this run.

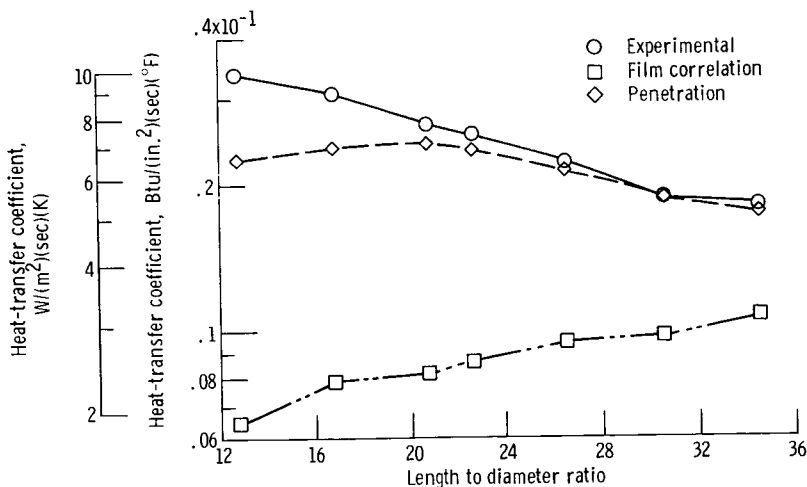


Figure 2. - Comparison of film penetration model and experimental heat-transfer coefficients.

Also shown in the figure is the heat-transfer coefficient prediction employing the penetration model concept (eq. (2)). For this particular run, the prediction agrees well with experiment. Incidentally, this run (3-1094) was not one of the original 11 runs used in determining the magnitude of the empirical constants. It does happen that the bulk fluid conditions are very close to critical for both temperature and pressure.

As a check on the versatility of the model to fluid state conditions far removed from the critical, high-pressure hydrogen data involving appreciable wall- to bulk-temperature ratios were included in the comparisons. Selected runs from references 26 and 27 were used for that purpose. Tables I and II are a listing of the run numbers and test section stations from references 25 to 27 and a tabulated comparison of the heat-transfer coefficients with the experimental values for hydrogen.

A quick observation of the series of graphs in figure 3 shows the relative merits of

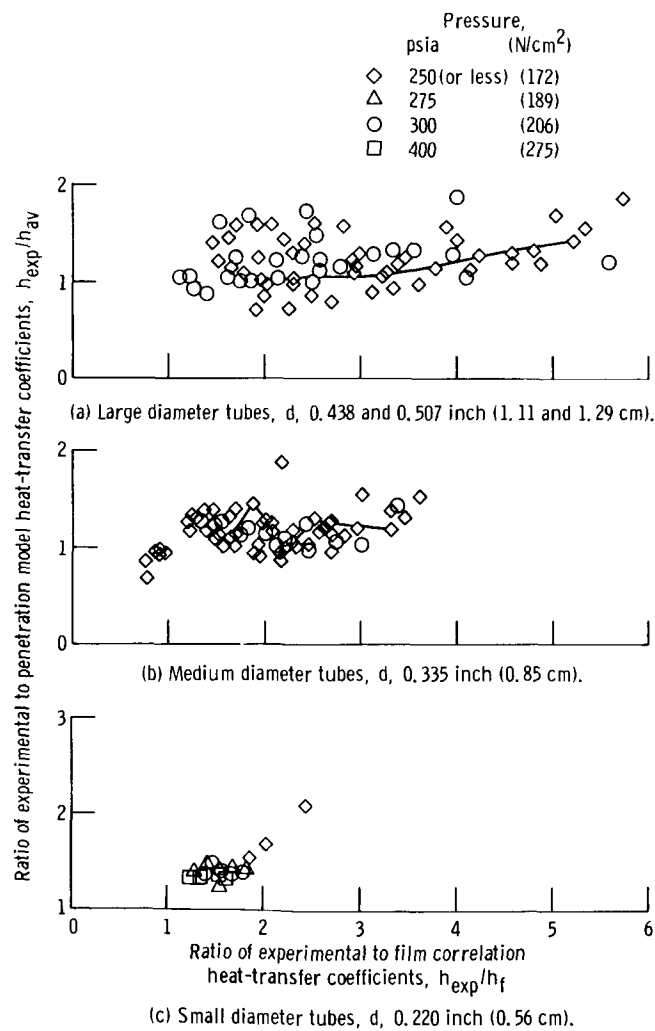


Figure 3. - Comparison of penetration model and film correlation predictions to experiment for cryogenic hydrogen.

TABLE I. - COMPARISON OF MODEL TO HYDROGEN EXPERIMENTAL INFORMATION

(a) Test section diameter, 0.507 inch (1.29 cm) (ref. 25)

Run	Axial distance to diameter ratio, L/D	Bulk pressure, P _b , psi	Wall temperature, T _w , °R	Bulk temperature, T _b , °R	Heat flux, q, Btu/(in. ²)(sec)	Bulk axial velocity component, U _b , ft/sec	Area fraction of penetration, A _p /A _t	Heat-transfer coefficient ratio		Penetration contribution fraction, $\left(\frac{h_p}{h_{av}}\right)\left(\frac{A_p}{A_t}\right)$
								h _{exp} /h _f	h _{exp} /h _{av}	
4-1093	12.8	250	305	59.8	0.91	46.4	0.093	5.75	1.81	0.71
	18.7	↓	391	61.6	↓	55.6	.101	3.98	1.26	.71
	22.6	↓	414	62.2	↓	64.1	.112	3.4	1.19	.68
	34.4	↓	539	64.6	↓	101	.124	2.0	.91	.60
5-1090	12.8	300	259	65.4	0.59	37	0.156	5.58	1.24	0.81
	18.7	↓	289	68.4	↓	40.9	↓	3.98	1.27	.73
	22.6	↓	394	71.5	↓	49.6	↓	2.56	.97	.68
	30.5	↓	489	80.9	↓	69.0	↓	1.73	.99	.52
*11-1101	12.8	450	323	64.3	0.93	39.9	0.113	5.19	2.14	0.62
	18.7	↓	362	66.7	↓	51.8	.137	3.82	1.75	.59
	22.6	↓	411	68.6	↓	61.9	.143	3.01	1.49	.56
	34.4	↓	529	78	↓	100.3	.147	1.79	1.15	.44
15-1091	12.8	450	379	58.2	0.59	37.6	0.052	2.13	1.23	0.45
	18.7	↓	432	61.6	↓	40.3	.063	1.85	.90	.54
	22.6	↓	477	63.5	↓	42.4	.067	1.67	.74	.58
	34.4	↓	497	68.5	↓	50.3	.092	1.46	.56	.64
*20-1092	12.8	500	282	70.5	0.59	22.1	0.139	3.99	1.18	0.74
	18.7	↓	300	75.6	↓	27.1	.156	3.31	1.02	.73
	22.6	↓	335	79	↓	31.1	.156	2.72	.96	.70
	34.4	↓	400	91.6	↓	45.6	.156	1.82	1.03	.52
3-1094	12.8	250	335	63	0.92	42.6	0.111	5.24	1.49	0.74
	18.7	↓	386	64.7	↓	56.2	.134	3.71	1.16	.72
	22.6	↓	430	66.1	↓	67.9	.141	2.94	1.07	.68
	34.4	↓	582	75	↓	112.3	.151	1.70	1.06	.46
2-1098	12.8	250	381	65.7	0.91	41.2	0.151	4.87	1.17	0.79
	18.7	↓	503	72.3	↓	63	.158	2.89	1.22	.63
	22.6	↓	561	79.6	↓	79.6	.158	2.32	1.29	.52
	34.4	↓	745	110.2	↓	132.3	.158	1.51	1.19	.33
23-1165	12.8	400	941	142.5	0.88	104.2	0.072	1.16	0.91	0.26
	18.7	↓	1057	158.5	↓	117.9	.087	1.02	.78	.29
	22.6	↓	1033	169.1	↓	126.8	.105	.99	.77	.29
	34.4	↓	892	199.1	↓	151.5	.158	.99	.84	.28
6-1088	12.8	250	255	60.5	0.6	35	0.09	5.36	1.53	0.73
	18.7	↓	269	62.3	↓	41	.12	4.56	1.27	.75
	22.6	↓	299	63	↓	46	.12	3.76	1.18	.74
	34.5	↓	391	65	↓	67.6	.14	2.17	.80	.68
7-1085	12.8	250	217	62	0.3	26	0.10	4.54	1.19	0.76
	18.7	↓	249	63	↓	31	.13	3.60	.97	.76
	22.6	↓	253	63.4	↓	35	.14	3.13	.88	.75
	34.5	↓	317	66	↓	49.5	.16	1.92	.67	.71
*26-1110	12.8	300	993	93.7	0.9	107	0.07	1.41	0.89	0.41
	18.7	↓	932	108	↓	131	.10	1.26	.91	.35
	22.6	↓	852	117.5	↓	161	.12	1.22	1.05	.24
	34.5	↓	757	147	↓	191	.16	1.12	1.10	.17

*Run numbers used in determining constants.

TABLE I. - Continued. COMPARISON OF MODEL TO HYDROGEN EXPERIMENTAL INFORMATION

(b) Test section diameter, 0.335 inch (0.85 cm) (ref. 25)

Run	Axial distance to diameter ratio, L/D	Bulk pressure, P _b , psi	Wall temperature, T _w , °R	Bulk temperature, T _b , °R	Heat flux, q, Btu/(in. ²)(sec)	Bulk axial velocity component, U _b	Area fraction of penetration, A _p /A _t	Heat-transfer coefficient ratio		Penetration contribution fraction, $\left(\frac{h_p}{h_{av}}\right)\left(\frac{A_p}{A_t}\right)$
								h _{exp} /h _t	h _{exp} /h _{av}	
1-880	19.5	250	697	64.6	2.39	105.6	0.100	3.28	1.17	0.67
	28.5	↓	960	70.0	↓	175.6	.103	2.35	1.06	.59
	34.5	↓	906	77.9	↓	240.2	.127	1.86	1.41	.33
	46.5	↓	835	105	↓	376.9	.158	1.38	1.40	.13
14-702	19.5	250	465	62.5	1.43	66.5	0.115	3.45	1.32	0.70
	28.5	↓	672	64.7	↓	99.8	.113	2.42	.87	.67
	34.5	↓	757	67.7	↓	133.4	.118	1.98	.90	.59
	46.5	↓	709	80.1	↓	216	.158	1.39	1.18	.26
16-700	19.5	275	432	59.1	1.50	84	0.078	3.00	1.55	0.52
	28.5	↓	572	62.4	↓	100.2	.084	2.47	1.09	.59
	34.5	↓	670	63.8	↓	117.4	.085	2.18	.95	.59
	46.5	↓	597	66.2	↓	167	.122	1.68	1.02	.45
*30-886	19.5	300	552	67.4	1.87	79.2	0.120	3.02	1.02	0.70
	28.5	↓	773	73.2	↓	121.6	.121	2.21	1.10	.52
	34.5	↓	870	80.9	↓	161.6	.129	1.83	1.20	.42
	46.5	↓	854	103.5	↓	252	.156	1.36	1.26	.20
*55-258	19.5	400	383	59.4	0.67	44.5	0.072	1.91	1.00	0.51
	28.5	↓	478	63.7	↓	49.8	.080	1.65	.71	.60
	34.5	↓	458	66.1	↓	54.4	.098	1.57	.67	.61
	46.5	↓	396	69.8	↓	65.8	.146	1.44	.71	.56
57-881	19.5	700	952	77.9	2.23	82.0	0.063	1.99	0.94	0.55
	28.5	↓	887	87.9	↓	105.9	.093	1.64	1.05	.41
	34.5	↓	819	94.9	↓	124.8	.117	1.45	1.06	.34
	46.5	↓	731	110.4	↓	165.3	.156	1.20	1.09	.22
4-888	19.5	250	898	68.7	2.23	120.9	0.104	2.85	1.12	0.64
	28.5	↓	1099	84.7	↓	202.2	.120	2.01	1.25	.44
	34.5	↓	1053	102.4	↓	271.5	.133	1.64	1.33	.29
	46.5	↓	1003	139.8	↓	402.7	.158	1.29	1.29	.15
3-887	19.5	250	628	63.2	2.51	111.9	0.088	3.32	1.39	0.62
	28.5	↓	889	65.7	↓	166.2	.088	2.57	1.13	.55
	34.5	↓	862	68.7	↓	222.5	.106	2.06	1.29	.43
	46.5	↓	737	79.9	↓	354.2	.158	1.46	1.39	.16
43-688	19.5	500	692	68.4	1.22	54.7	0.063	2.01	0.84	0.61
	28.5	↓	771	74.6	↓	70.0	.078	1.72	.71	.62
	34.3	↓	662	78.6	↓	87.6	.10	1.49	.77	.53
	46.3	↓	550	87.5	↓	111	.14	1.24	.94	.35
47-653	19.5	400	694	60.2	1.3	86.1	0.04	1.79	1.11	0.40
	28.4	↓	642	64.7	↓	97.8	.06	1.64	.95	.45
	34.3	↓	553	67.0	↓	107.2	.075	1.56	.95	.44
	46.3	↓	464	70.5	↓	130.3	.10	1.40	1.00	.36
32-312	19.4	325	455	63.9	1.82	75	0.098	3.37	1.44	0.61
	28.35	↓	685	67.7	↓	104	.096	2.48	.97	.64
	34.3	↓	759	75.2	↓	171	.118	1.75	1.15	.42
	40	↓	666	88.5	↓	252	.135	1.32	1.25	.18
34-273	19.4	400	595	63.1	1.82	94.7	0.058	2.38	1.45	0.42
	28.3	↓	585	69.3	↓	124	.087	1.97	1.20	.44
	34.3	↓	567	70.5	↓	133.6	.097	1.87	1.21	.42
	40	↓	473	75.4	↓	203.8	.131	1.58	1.32	.27

*Run numbers used in determining constants.

TABLE I. - Concluded. COMPARISON OF MODEL TO HYDROGEN EXPERIMENTAL INFORMATION

(c) Test section diameter, 0.22 inch (0.56 cm) (ref. 25)

Run	Axial distance to diameter ratio, L/D	Bulk pressure, P_b , psi	Wall temperature, T_w , °R	Bulk temperature, T_b , °R	Heat flux, q , Btu/(in. ²)(sec)	Bulk axial velocity component, U_b , ft/sec	Area fraction of penetration, A_p/A_t	Heat-transfer coefficient ratio		Penetration contribution fraction, $\left(\frac{h_p}{h_{av}}\right)\left(\frac{A_p}{A_t}\right)$
								h_{exp}/h_f	h_{exp}/h_{av}	
3-1022	29	300	748	67.1	2.87	283	0.076	1.78	1.38	0.28
	36	↓	690	69.3	↓	355.7	.097	1.55	1.39	.19
	45	↓	601	73.8	↓	473.1	.135	1.36	1.39	.09
9-1043	29	225	201	56.9	0.76	141.1	0.083	2.42	2.11	0.19
	36	↓	265	57.9	↓	146.7	.077	1.88	1.54	.23
	45	↓	315	59.1	↓	155.3	.080	1.55	1.23	.25
11-1026	29	300	775	78.2	2.87	231	0.09	1.63	1.36	0.26
	36	↓	732	84	↓	286	.117	1.42	1.34	.18
	45	↓	660	94	↓	367	.156	1.24	1.32	.10
*22-1029	29	700	851	83.7	2.88	147	0.069	1.48	1.20	0.24
	36	↓	712	93.4	↓	187	.111	1.25	1.18	.16
	45	↓	667	100.5	↓	217	.139	1.21	1.19	.14
5-856	29	400	783	70.7	3.3	196	0.068	1.96	1.45	0.31
	34	↓	688	76.2	↓	269	.142	1.60	1.41	.20
	45	↓	635	83.3	↓	363	.156	1.34	1.36	.10
30-1038	23	700	178	61.2	1.39	150.2	0.109	1.56	1.67	0.03
	33	↓	197	65.1	↓	158.9	.137	1.49	1.62	.10
	40	↓	191	67.4	↓	165.4	.158	1.52	1.69	.06
20-1036	23	400	187	59.3	1.35	184	0.088	2.12	2.18	0.06
	33	↓	244	61.8	↓	196	.095	1.75	1.73	.10
	40	↓	226	63.3	↓	205	.12	1.83	1.84	.10
4-1007	29	275	490	62.2	1.41	165	0.064	1.62	1.24	0.28
	36	275	481	63.1	1.41	182	.077	1.53	1.18	.28
2-1005	29	275	774	68.9	2.71	251	0.082	1.83	1.37	0.31
	36	↓	708	70.6	↓	286	.095	1.56	1.42	.19
	45	↓	630	80.5	↓	439	.13	1.34	1.39	.09
14-1025	29	400	722	72	2.88	219	0.073	1.67	1.32	0.27
	36	↓	679	75.1	↓	262	.091	1.50	1.30	.21
	40	↓	594	79.8	↓	330	.11	1.35	1.33	.12

*Run numbers used in determining constants.

the model in predicting convective heat transfer for near-critical hydrogen as compared to the conventional forced convection correlation. The three graphs shown segregate the results according to tube diameter - large, medium, and small. This is the same as segregating the data according to ranges of free stream velocity. The magnitudes of free stream velocities were inversely proportional to the test section diameters. The ordinates are ratios of the experimental heat-transfer coefficients to the predicted coefficients from the model. The abscissas of the figures are the ratios of the experimental heat-transfer coefficients to the coefficients predicted by the conventional Dittus-Boelter type correlation. The most dramatic results are associated with the large tube diameter data. Extremely large ratios of experimental heat-transfer coefficient to film correla-

TABLE II. - HIGH-PRESSURE HEAT-TRANSFER DATA

(a) Test section diameter, $d = 0.21$ inch (0.53 cm) (ref. 27)

Run	Axial distance to diameter ratio, L/D	Bulk pressure, P_b , psi	Wall temperature, T_w , °R	Bulk temperature, T_b , °R	Heat flux, q , Btu/(in. ²)(sec)	Bulk axial velocity component, U_b , ft/sec	Area fraction of penetration, A_p/A_t	Heat-transfer coefficient ratio		Penetration contribution factor, $\left(\frac{h_p}{h_{av}}\right)\left(\frac{A_p}{A_t}\right)$
								h_{exp}/h_f	h_{exp}/h_{av}	
5	9.5	1000 ↓	1326	82.7	12.4	291	0.03	2.30	2.10	0.12
	19		1296	100.1	11.9	394	.06	1.82	1.72	.11
	28.6		1030	118	10.98	521	.09	1.55	1.60	.07
	38		855	137	10.7	654	.14	1.45	1.62	.04
6	9.5	1000 ↓	864	74.6	9.7	279	0.04	2.19	2.15	0.05
	19		1253	87.8	10.4	346	.05	1.76	1.62	.12
	28.6		980	100.6	9.4	438	.08	1.53	1.52	.09
	38		773	113.5	9.0	544	.12	1.42	1.54	.04
28	9.5	1250 ↓	1093	81.7	10.2	208	0.04	2.18	2.01	0.11
	19		1370	100.6	10.9	265	.06	1.80	1.60	.16
	28.6		806	119.2	10.2	337	.13	1.85	1.97	.07
	38		847	137	9.3	412	.06	1.47	1.63	.06
35	9.5	550 ↓	1378	70.3	7.4	224	0.03	2.46	1.83	0.27
	19		954	79	6.6	299	.06	2.11	1.78	.20
	28.6		755	87.7	6.2	405	.09	1.76	1.77	.09
	38		663	97.7	5.7	527	.13	1.44	1.55	.05

(b) Test section diameter, $d = 0.22$ inch (0.56 cm) (ref. 26)

206-A-6	21	1450 ↓	930	92	5.6	189	0.06	1.31	1.22	0.13
	26		904	99	↓	205	.08	1.26	1.19	↓
	30.8		961	106	↓	221	.08	1.18	1.11	↓
103-A-4	14.3	750	957	143	1.9	121	0.07	1.23	1.04	0.21
	17.5	750	1098	151	1.9	130	.07	1.11	.92	.23
230-A-6	21	1500	708	126	5.6	221	0.08	1.21	1.27	0.04
	28	1500	659	133	5.6	281	.10	1.18	1.26	.04
*388-A-7	17.1	1350	442	87	0.9	34	0.09	1.28	0.94	0.33
	19.4	1350	471	89	.9	35	.09	1.21	.86	.35

(c) Test section diameter, $d = 0.335$ inch (0.85 cm) (ref. 26)

171-A-4	20.6	900 ↓	323	67	2.8	209	0.07	1.47	1.53	0.03
	30.2		388	72	↓	225	.08	1.24	1.28	.05
	33.4		351	74	↓	231	.10	1.31	1.37	.05

*Run numbers used in determining constants.

tion coefficient were observed. The relatively small magnitude of velocity in the large tubes probably enabled the penetration mechanism to go on relatively unabated by free stream momentum effects. If one judges from figure 3(a) (large diameter tubes), it does appear that the penetration model concept is quite successful in reducing the differences between experimental and predicted values of the heat-transfer coefficient. Similar, but

lesser, improvements in the prediction of the heat-transfer coefficients were observed with smaller diameter tubes (figs. 3(b) and (c)).

An appreciation of the relative magnitude of the penetration mechanism contribution to the overall heat-transfer mechanism can be discerned from figure 4, which compares the ratio of the heat flux contribution ascribed to penetration to the average overall heat flux with the ratio of the experimental heat-transfer coefficient to the film coefficient. Over a considerable range of conditions, the relative contribution of the penetration mechanism does increase as the ratio of the experimental heat-transfer coefficient to the film coefficient increases. The relative contribution of the penetration mechanism appears to peak at approximately 80 percent of the predicted average heat-transfer rate. Note that the near-critical pressure data make up the high end of the plot.

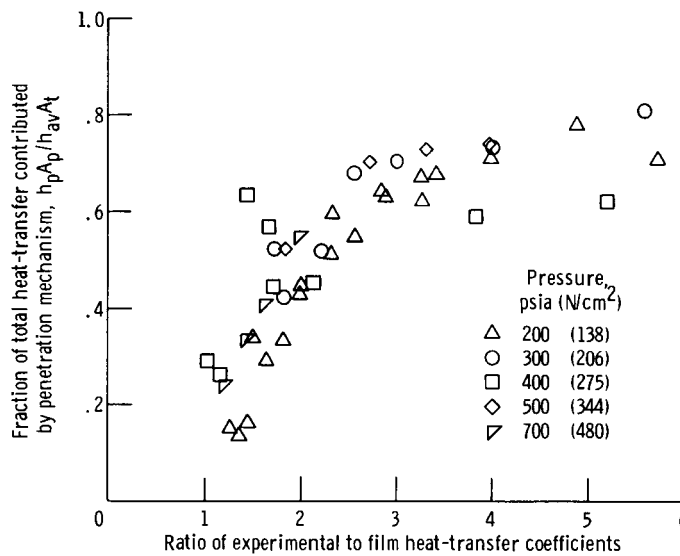


Figure 4. - Relative contribution of penetration mechanism to overall heat transfer.

The reader may wonder if this figure just constitutes a sort of back-calculation display of some of the empirical aspects of the model. It is true that the magnitudes of the coefficient in equation (A7) (expression for h_p) and C_3 in equation (A9) (expression for A_p/A_t) were determined from comparisons with a few sample runs. After fixing these constants, equations (A7) and (A9) were applied to a large array of hydrogen data over a considerable range of conditions. Computed parameters, such as the penetration coefficient h_p , varied over one order of magnitude. Thus, the author claims that the method applies to a broad range of conditions where density effects, primarily, alter the conventional representation of turbulent forced convection.

The correlation equation was further compared to some high pressure, high heat flux data for liquid hydrogen presented in references 26 and 27. The pressure of the liquid hydrogen was well above critical, but the temperature was around critical. For these conditions, gradients in density and transport properties are not as severe as near the critical point.

Table II is a tabulation of the predicted heat-transfer coefficients compared to the experimental values of references 26 and 27. Again the conventional film correlation and the penetration model correlations are presented. One can conclude for these data that the film correlation and the correlation involving the penetration model predict about the same values. The reason for this is that the penetration component for these supercritical pressures is small. Thus, the "average" coefficient is principally the film coefficient (see eq. (2)).

Carbon Dioxide and Water

A limited comparison of the model predictions with experimentally determined heat-transfer data was made for carbon dioxide and water. Data from references 8 and 9 were utilized. The information on the run numbers and comparisons of the predictions to experimental values are presented in table III. The empirical constants derived from the hydrogen calculations were employed in the computational procedures for these fluids.

Regarding the carbon dioxide data, the experimental heat fluxes are very low and the ratios of wall to bulk temperatures are also very low. The experimental data points were obtained at one station in the test section. The runs selected included data with bulk temperatures above and below the critical value.

Actually, the operating pressure was slightly above the critical pressure, so the bulk temperature range represents conditions below the transposed critical temperature (loci of maximum C_p) and at the transposed critical temperature. For runs 23 and 25 the bulk temperature was less than the critical value and there appears to be no enhancement of the heat transfer. When experimental conditions were altered such that the bulk temperature was essentially at the transposed critical value, the heat-transfer coefficient reached a maximum value. However, the predicted film correlation coefficient was far below the experimental value. The introduction of a penetration component improved the prediction considerably as is evident from an examination of runs 28 and 30.

About all that can be concluded from this comparison with experimental carbon dioxide heat-transfer data is that several experimental data points were predicted fairly well by the analysis. For these cases the predictions were generally superior to estimates obtained from pipe flow correlations. Also, the empirical constants of the model, which were derived from hydrogen data, appear to be applicable to another fluid.

TABLE III. - COMPARISON OF MODEL TO EXPERIMENTAL INFORMATION FOR CARBON DIOXIDE AND WATER

(a) Fluid, carbon dioxide; test section diameter, d = 0.9 inch (2.3 cm) (ref. 8)

Run	Axial distance to diameter ratio, L/D	Bulk pressure, P _b , psi	Wall temperature, T _w , °F	Bulk temperature, T _b , °F	Heat flux, q, Btu/(in. ²)(sec)	Bulk axial velocity component, U _b , ft/sec	Area fraction of penetration, A _p /A _t	Heat-transfer coefficient ratio		Penetration contribution factor, $\left(\frac{h_p}{h_{av}}\right)\left(\frac{A_p}{A_t}\right)$
								h _{exp} /h _f	h _{exp} /h _{av}	
23	30.8	1075	92.9	83.3	0.072	13.7	0.156	0.66	0.71	0.45
25	↓	↓	94.0	85	↓	13.7	↓	1.61	1.60	.11
28	↓	↓	98.7	87	↓	13.7	↓	3.70	2.55	.39
30	↓	↓	133	88.8	↓	16.4	↓	2.14	.91	.64

(b) Fluid, water; test section diameter, d = 0.371 inch (0.94 cm) (ref. 9)

23200	40	4000	887	731	1.05	16.9	0.156	2.37	0.74	0.74
23202	73	4000	922	738	1.05	18.9	.156	2.23	.73	.72
23206	137	4000	904	749	1.06	25	.156	2.04	1.19	.51
22108	40	3300	832	691	.57	7.6	.14	3.31	.42	.89
22112	120	3300	820	704	.57	10	.14	3.24	.58	.85
22114	137	3300	810	707	.58	11.4	.156	3.09	.61	.83
22445	57	3300	923	702	0.37	4.0	0.156	3.56	0.10	0.97
22453	186	↓	1131	725	.39	10.6	.156	1.33	.26	.83
22461	120	↓	731	700	1.31	3.6	.156	1.72	.38	.80
22431	25	↓	932	687	.76	7.4	.10	3.66	.38	.90
22134	73	↓	1111	703	.77	9.6	.145	2.67	.16	.95
22874	8	↓	746	719	.15	41	.03	2.29	2.1	.08
22875	24	3300	747	720	0.15	41	0.07	2.22	1.9	0.19
22876	40	3300	752	721	.15	41	.10	1.99	1.65	.25
22877	57	3300	755	722	.15	41	.11	1.89	1.55	.26
23222	8	4000	787	747	.24	27	.032	2.39	1.99	.19
23223	24	4000	791	748	.24	28	.076	2.25	1.51	.38
23224	40	4000	796	749	.24	28	.11	2.07	1.21	.48
23225	57	4000	800	751	0.24	29	0.11	1.95	1.14	0.48
22898	8	3300	806	720	.34	35	.04	4.57	2.70	.43
22899	25	↓	819	723	↓	40	.08	4.13	2.0	.55
22900	40	↓	834	726	↓	45	.12	3.70	1.79	.57
22901	57	↓	846	730	↓	50	.13	3.43	1.96	.50

The near-critical water heat-transfer data from reference 9 were utilized in a comparison. The authors of reference 9 correlated their data by a regression technique and suggested the following correlation equation:

$$\frac{hd}{k_i} = 0.00459 \left(\frac{DG}{\mu_i}\right)^{0.923} \left[\frac{(H_i - H_b)}{(T_i - T_b)} \frac{\mu_i}{k_i}\right]^{0.613} \left(\frac{v_b}{v_i}\right)^{0.231} \quad (6)$$

where H is enthalpy, v is specific volume, and the subscripts i and b refer to inside wall conditions and bulk conditions, respectively. They claimed that this form of convective correlation enabled better comprehension of the widely varying physical and trans-

port properties than the traditional pipe flow correlation wherein properties are evaluated at some reference condition.

It is interesting to note that the near-critical water heat-transfer data exhibit the same trends as the hydrogen and carbon dioxide data: that is, the experimental heat-transfer coefficient is always greater than the predicted value based on film properties.

Several runs from reference 9 are tabulated in table III(b) and the data are compared to the penetration contribution model. For the low velocity runs ($u < 10$ fps), the penetration model overpredicted severely. For the higher flow velocities, the penetration model underpredicted, but generally the degree of underprediction was less than what the film correlation provided.

It cannot be claimed that the penetration model presented herein is a satisfactory means of predicting the near-critical water heat-transfer data of reference 9. Nevertheless, the trends of enhancement do seem to be in agreement with the penetration explanation.

APPLICATION OF PENETRATION MODEL TO TWO-PHASE HEAT TRANSFER

One two-phase flow regime which appears applicable to the penetration model is mist flow. Tiny liquid droplets migrate transversely from the bulk to the wall where they appear to participate in conduction and evaporation mechanisms. These migrating droplets can be considered to be penetration packets.

The heuristic model which was developed for the near-critical fluid was applied to experimental mist flow data. The same equations and constants were utilized except for the area fraction parameter. The area fraction was calculated from estimates of the liquid void fraction computed in reference 28. Also, a film density was utilized which was weighted with the mass fraction of liquid and vapor at film conditions. This reference density labeled ρ_{fm} was defined to be

$$\rho_{fm} = \frac{1}{\frac{x}{\rho_{fg}} + \frac{1-x}{\rho_b}} \quad (7)$$

where x is the estimated average quality, ρ_{fg} is gas density evaluated at film temperature, and ρ_b is liquid density.

With the exception of these modifications, the approach employed for the near-critical fluids was applied to the two-phase problem. The correlation coefficients were

identical when equations (A3) and (A4) were employed. Figure 5 compares the estimate involving the penetration model with the film correlation approach. It is apparent that the penetration model contribution improves the comparison with experimental results.

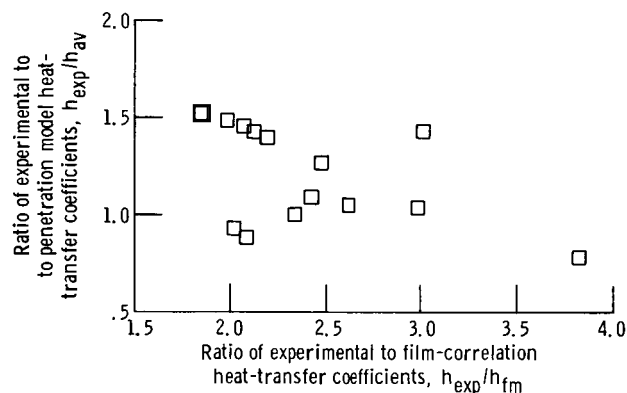


Figure 5. - Comparison of penetration model for two-phase hydrogen to single-phase correlation. Diameter, d , 0.375 inch (0.95 cm).

CONCLUSIONS

Notwithstanding the empirical nature of the description of the penetration mechanism, it does appear that the inclusion of such a component in a convective heat-transfer mechanism helps to explain the dramatic changes in heat transfer observed with near-critical fluids. It is further concluded that the peculiar heat transfer of this regime appears to be associated with the nature of the turbulence structure of the near-wall region. Fluid properties are important in the penetration mechanism. In particular, density and the rate of change of density of expansion mechanistically determine the frequency of the penetration cycle. Thus, a sizeable portion of the influence on overall heat transfer by fluid properties is carried into the analysis as a mechanistic effect.

Recognition of the time-unsteady contribution to the heat transfer does emphasize that some comprehension of the instantaneous heat-transfer processes be achieved before any statistical averaging be done. The importance of assessing various mechanistic effects before averaging was also observed in studies of nucleate boiling (ref. 29). In the development of the standard turbulent flow heat-transfer correlations, time-averaged values of velocity and temperature are introduced initially. The mechanism is treated as a time-steady phenomenon which utilizes average values to comprehend the turbulent behavior.

The model presented herein suggests that the heat-transfer mechanisms of the near-critical fluid and two-phase fluid (boiling) are similar in some respects. Such a similarity was suggested several years ago, and it has had experimental verification through

visualization techniques. It does seem that with further refinements a unified model of turbulent convection is possible for all the fluid states. This would obviate the current practice of abruptly changing heat-transfer models when the boundaries of fluid states are crossed.

Finally, the model portrayed herein is a first approximation to a mechanism that has been qualitatively discerned experimentally. It is presented as one heuristic model to explain an enhanced component of heat transfer. Detailed information on the sublayer structure is needed to produce better quantitative data for verification and refinement of the model. The comparison of experimental data with a predicted heat-transfer coefficient, which included a penetration contribution, was presented to support the arguments for the model proposed and not to propose another heat-transfer correlation.

Lewis Research Center,
National Aeronautics and Space Administration,
Cleveland, Ohio, August 29, 1969,
129-01.

APPENDIX A

HEURISTIC MODEL OF TURBULENT TRANSPORT WITH PENETRATION COMPONENT

Penetration Heat-Transfer Coefficient

The key concept in formulating the model of the penetration component of the boundary layer is borrowed from the literature dealing with the heat transfer in fluidized beds. The picture of a discrete fluid packet migrating toward the wall, as shown in figure 1, is similar to the model used in reference 30, for instance, to estimate the heat transfer between a fluidized bed and the vessel contact surfaces. As pointed out in the INTRODUCTION, Hanratty (ref. 19) must be credited with suggesting that such a penetration concept, which was originally applied to mass diffusion, could be applied to the turbulent boundary layer.

For the estimation of h_p , it is assumed that the packet penetrating to the wall carries its bulk properties and then begins its transient conduction while in contact with the wall. Since it is in the beginning moments of the conduction transient that most of the heat transfer is contributed, the initial bulk properties of the fluid are inserted in the expression for the transient heat flux. The familiar expression for transient conduction is

$$\frac{\partial^2 T}{\partial y^2} = \frac{1}{\alpha} \frac{\partial T}{\partial \tau} \quad (A1)$$

For the boundary conditions applicable to a very thick slab

$$\tau = 0 \quad T = T_\infty$$

$$y = 0 \quad T = T_w$$

$$y = \infty \quad T = T_\infty$$

the solution to equation (A1) for a statistical average time period τ_c can be shown to be

$$q_p = \frac{2}{\sqrt{\pi}} \sqrt{\frac{k\rho C}{\tau_c}} (\Delta T) \quad (A2)$$

and the heat-transfer coefficient h_p is

$$h_p = \frac{2}{\sqrt{\pi}} \sqrt{\frac{(\kappa \rho c_p)_b}{\tau_c}} \quad (\text{A3a})$$

Alternatively, equation (A3a) can be expressed as

$$h_p = \frac{2}{\sqrt{\pi}} \sqrt{\omega (\kappa \rho c_p)_b} \quad (\text{A3b})$$

where ω is the frequency.

The principal unknown in equation (A3a) is the contact time τ_c (or ω). From a more detailed look at the mechanics of the penetration of a bulk fluid packet to the wall, one can gain an insight into parameters influencing the contact time τ_c . The stages in the life of a packet as it comes to the wall and departs are shown in figure 6. The events

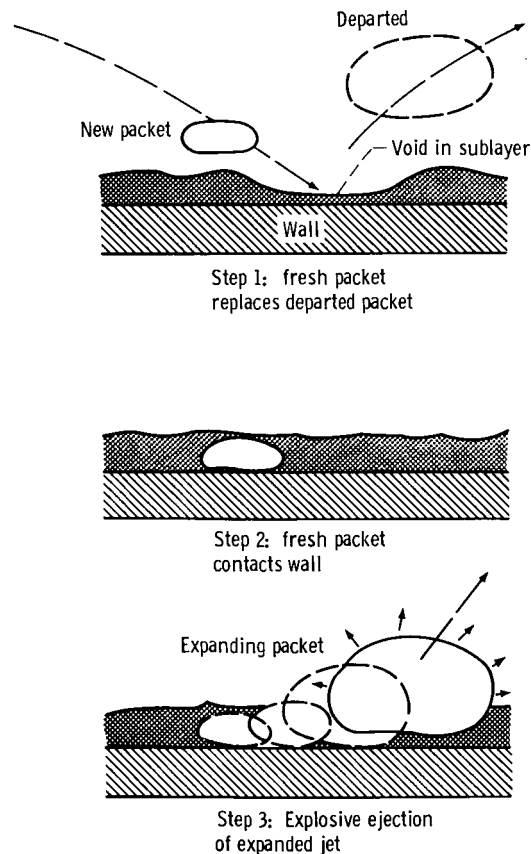


Figure 6. - Stages in life of penetration packet.

shown in figure 6 begin immediately following the departure of a packet from the wall region. Its departure leaves a void which is immediately occupied by a new packet from the outer edge of the boundary layer. This is step 1 of figure 6.

Step 2 is envisioned to be the filling of the void in the sublayer by a packet of fluid from the bulk region. The turbulent mixing inherent to the flow is sufficient to cause the void to be filled.

The final step in the process is the rapid expansion of the fluid packet while in contact with the wall. The packet retains its identity and expands as a unit while soaking up heat from the wall. Only a very short contact time would be required for the entire packet to respond to the wall temperature environment. If the dimensions of a packet approximate the sublayer thickness (2×10^{-3} in. or 5×10^{-3} cm) the relaxation time for a temperature disturbance to propagate over that thickness would be less than 10^{-6} second.

The explosive-like expansion of the packet as it is heated from a near-critical thermal state to a temperature condition approximating wall conditions induces the inertial motion of fluid surrounding the packet. These inertial effects are considered to be the source of the jetting action that creates a void or hole in the sublayer region whereupon the replenishment cycle repeats again.

From the qualitative description of the penetration mechanism presented thus far, the following intuitive arguments are presented in order to develop a parametric expression for the penetration frequency. At the outset it is important to realize that the prime mover of the penetration model is rapid expansion by heating. Expansion amplifies a disturbance in the sublayer to enable a local mass exchange. It would be difficult for the thermal disturbance to make its influence felt in a high-speed flow. This would be analogous to the observance of the influence of a film cooling jet on a boundary layer. The faster the free stream traveled, the less "effective" or influenced would be a transverse film jet of a fixed strength. Consequently, the frequency of penetration would be inversely proportional to the momentum in the free stream - for example, a product of the film density and free stream velocity. This intuition may appear to contradict the familiar notion that turbulence in a flowing fluid is strengthened as the flow rate (Reynolds number) increases. In this model being proposed, I am assuming that the penetration transport is effected by an explosive-like thermal expansion of a fluid packet located in the sublayer. The local disruption of the sublayer can be viewed as an instability. I am saying that the higher shear associated with higher flow rates tends to dampen a thermal instability, thereby inhibiting the penetration mechanism. On the other hand, the magnitude of expansion possible within the boundary layer would be an index of the penetration frequency. This could be portrayed by a density difference between bulk and wall conditions.

In order to compare the expansion property of the boundary layer with the axial momentum, the two effects should be made dimensionless in a parametric form. Since the effects are competitive, it is convenient to cast them into a ratio form with the

expansion term as the numerator. Included in the expansion parameter is a theoretical expansion velocity, which could result from perfect conversion of thermal energy into kinetic energy $(\sqrt{2J_{gc}(H_w - H_b)})$.

Since this expansion process occurs within a boundary layer, it seems appropriate to include viscosity terms in the parameter. The evaluations of the viscosity terms are made consistent with the density evaluation. Consequently, the ratio takes on the nature of a Reynolds number ratio:

$$a = \frac{(\rho_b - \rho_w) \sqrt{2J_{gc}(H_w - H_b)}}{\rho_f U_\infty} \frac{\mu_f}{\mu_b} \quad (A4)$$

As was mentioned in the section PROPOSED HEAT-TRANSFER MODEL the previous dimensionless ratio modifies an adiabatic frequency ω_0 (see eq. (4)), and can be interpreted to be a frequency enhancement factor. The magnitude of ω_0 was determined empirically, but its value was observed to approximate measured sublayer oscillation frequencies. The value of ω_0 used was approximately 20 cps.

The form of equation (4) suggests that the penetration contact time is relatively long (low frequency) when the magnitude of the free stream momentum overpowers the expansion mechanism. A long contact time signifies an ineffective penetration mechanism or preservation of the sublayer. The ejection mechanism is primarily dependent on a large density change in the packets which penetrate to the wall. In addition, the effectiveness of this ejection mechanism is related to the heat flux level. This is portrayed by the enthalpy-difference term under the radical. Very large heating rates or extreme density changes, or a combination of both, lead to short contact times. The shorter the contact time, the greater the frequency of the penetration mechanism, which results in an improved heat-transfer coefficient.

It is interesting to observe that the amplification ratio in equation (4) is similar to one of the principal terms found in a stability analysis of a fluidized bed (ref. 32). The similarity of the penetration mechanism within the boundary layer to the mechanism of heat transport in a fluidized bed has been cited before in this report. Stability criteria for the fluidized bed as found in reference 31 are a further example wherein some similitude exists. Ruckenstein (ref. 32) suggested the pertinence of the study in reference 31 to the penetration model of the turbulent boundary layer. Reference 32 contains a well-developed discussion of the penetration model and compares it to the more conventional time-averaged boundary layer model.

Substituting the expression for frequency (eq. (4)) into the equation (eq. (A3a)) for the heat-transfer coefficient yields the useable form for heuristic comparisons with experimental data:

$$h_p = \sqrt{\frac{\omega_o}{\pi} (k\rho c_p)_b \frac{(\rho_b - \rho_w)}{\rho_b U_\infty} \sqrt{2g_c J(H_w - H_b)} \frac{\mu_f}{\mu_b}} \quad (A5)$$

As was mentioned earlier, the reference frequency ω_o was treated as an empirical constant.

Distribution of Penetration Areas

The question does arise concerning the distribution of the areas representing the two heat-transfer mechanisms. In order to get some estimate of the distribution of the penetration areas on the surface, a simple model of the penetration mechanisms was considered. The model assumed that the penetration mechanism was analogous to the penetration of a wall jet into a channel flow. The behavior of wall jet trajectories introduced normal to channel flow was studied in reference 33 and an empirical expression for the penetration distance was correlated. The principal dependency of the penetration distance was with the ratio of the wall jet velocity to the free stream velocity. Using the Gordier correlation made it possible to develop an expression for the penetration of a thermal jet into the fluid stream. Perhaps the key observation in formulating the analogy to Gordier's jet model is the fact that the Stanton number $q/\rho \Delta H U$ can be interpreted as a ratio of two orthogonal velocities. The numerator $q/\rho \Delta H$ represents a velocity normal to the wall and the denominator is the free stream velocity U . Such an interpretation of the Stanton number as it applies to two-phase and near-critical forced convection is found in reference 25. For two-phase systems, it is often referred to as the Sterman parameter.

The expression for penetration distance derived in appendix B and normalized with respect to a characteristic channel dimension is

$$\frac{y_p}{D} = C_2 Re_d^{-0.2} \left(\frac{L}{D}\right)^{0.8} (St)_b^{0.8} \quad (A6)$$

In the interpretation of this dimensionless number, it is assumed that it represents the distance traveled by fluid packets as they migrate toward and away from the wall. In the derivation, only the motion away from the wall was considered.

The penetration area A_p (see fig. 1) would be directly related to the penetration distance y_p . It seems reasonable to assume that a minimal y_p/D exists, which is a threshold of the thermally induced penetration mechanism. The penetration area fraction of the total surface would increase with an increase in the dimensionless penetration dis-

tance. A relation between the area fraction of penetration A_p/A_t and y_p/D was found empirically. Initially, the relation between these parameters was assumed to be of the form

$$\frac{A_p}{A_t} = C_5 \left(\frac{y_p}{D} \right)^n \quad (A7)$$

As a first guess, the exponent n was assumed to be one. It turned out through comparison of a limited amount of experimental data (11 runs) with the equation representing the overall model that this first approximation was a good one. Thus, the penetration area fraction can be represented by

$$\frac{A_p}{A_t} = C_6 \left(St_b \frac{L}{D} \right)^{0.8} Re^{-0.2} \quad (A8a)$$

The weak dependency on Re was dropped from the equation. Equation (A8a) was used in the form

$$\frac{A_p}{A_t} = C_7 \left(St_b \frac{L}{D} \right)^{0.8} \quad (A8b)$$

for values of $St(L/D) < 0.03$.

The magnitude of the coefficient C_7 was determined to be 2.8 by using a sample set of hydrogen runs. Figure 7 illustrates how equation (A8b) compares to the empirical check of the sample data. In all of the calculations presented herein, the value of C_7 was fixed at the value of 2.8.

As is observed in figure 7, the area fraction A_p/A_t appears to maximize at a value of 0.16 and then to level off for the upper ranges of the $St(L/D)$ parameter. This is somewhat analogous to what happens on boiling surfaces near burnout where the liquid-wetting area reaches some maximum fraction of the total area. Up to that point the wetting area is a function of the average heat flux (see ref. 34).

As a further comparison of the effect of a flow rate normal to a wall interacting with the principal flow along a wall, some transpiration heat-transfer data were utilized. Wall suction by means of a transpiration surface can be considered to be a physical representation of the penetration model presented herein. Certainly by suction, species of the free stream flow are carried through the boundary layer to the wall where their free stream molecular properties influence thermal exchange at the wall. In this respect, the suction

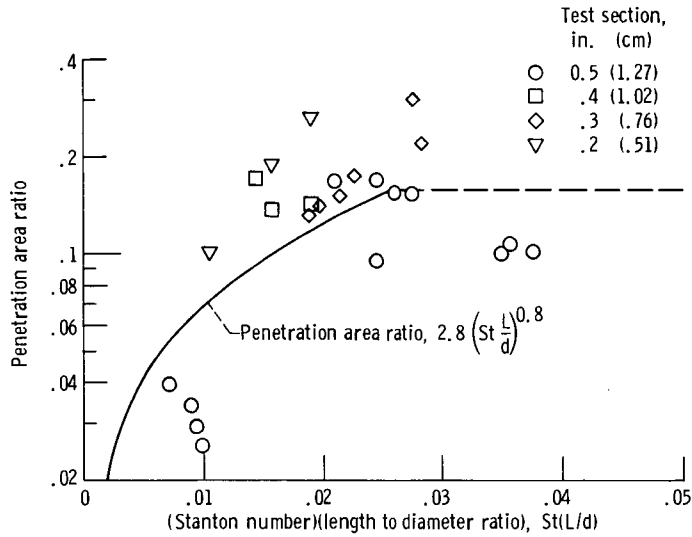


Figure 7. - Penetration area fraction as function of Stanton number and length to diameter ratio.

process enhances heat exchange at the wall. Indeed, measurements of turbulent heat transfer with suction show dramatic enhancements over comparable conditions with no suction. This has been clearly demonstrated in the data of reference 35 and other similar experiments. Figure 8, which is taken from reference 35, shows that the ratio of the transpired mass flow to the total mass flow was almost directly proportional to the change in Stanton number at a fixed L/D . Since the ratio of transpired flow to total flow can be interpreted to represent the penetration area fraction, the use of the transpiration data lends support to the functional relation of equation (A8b).

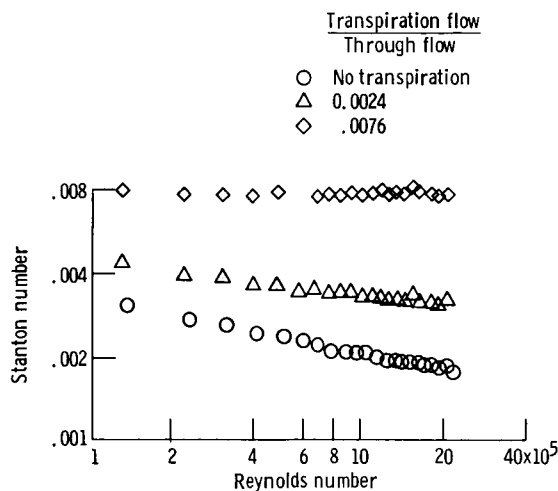
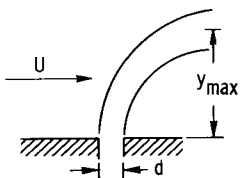


Figure 8. - Effect of transpiration flow (suction) on local heat transfer (from ref. 35).

APPENDIX B

PENETRATION DISTANCE

If it is assumed that the penetration distance associated with a fluid packet leaving the wall is analogous to the penetration distance of a jet into a fluid stream, then a rather simple relation for penetration distance can be developed. One experimental study of jet penetration normal to a flowing stream is contained in reference 33. The maximum jet penetration distance was observed to be a function of a ratio of the jet velocity to the free stream velocity. In terms of the parameters of the accompanying figure, the equation for maximum penetration distance is



$$\frac{y_{\max}}{d} = C_8 \left(\frac{v}{U} \right)^n \quad (\text{B1})$$

The author of reference 33 suggested that n was 0.74.

It is assumed that the thermal penetration distance of a packet of fluid leaving the wall can be correlated by the same type of equation as equation (B1). Instead of a jet nozzle diameter d , the normalizing parameter is the thermal layer thickness. It is assumed that the cross-section dimension of the fluid jet emanating from the wall is of the order of the thermal layer thickness. Rewriting equation (B1) as it applies to the thermal penetration distance and with a thermal layer thickness parameter:

$$\frac{y_{\max}}{\varphi} = C_9 \left(\frac{v}{U} \right)^n \quad (\text{B2})$$

For simplicity n is assumed to be 0.8. The term v/U can be evaluated in several ways. One way is to recognize that $v/U = f(\text{St}) = q/\Delta H \rho U$ where ΔH is enthalpy difference between wall and bulk condition. Modifying equation (B2) to include channel height yields

$$\frac{y_{\max}}{D} = C_{10} \frac{\varphi}{D} (\text{St})^{0.8} \quad (\text{B3})$$

For a constant q surface, a simplified treatment of the integral energy equation in axisymmetric coordinates yields the energy thickness (information obtained from a private communication with D. R. Boldman of Lewis) as follows:

$$\frac{\varphi}{D} = 0.031 \text{Re}_d^{-0.2} \left(\frac{L}{D}\right)^{0.8} \quad (\text{B4})$$

Equation (B4) depicts the development of the thermal layer in the entrance region along a flat plate or along a tube. Experimental studies have shown that the thermal entrance effects may persist as far down as $L/D = 40$. Substitution of equation (B3) into (B4) yields

$$\frac{y_p}{D} = C_{11} \text{Re}^{-0.2} \left(\frac{L}{D}\right)^{0.8} (\text{St})^{0.8} \quad (\text{B5})$$

This equation is assumed to retain the L/D correction up to values of $L/D = 40$. Thereafter, the L/D correction is held constant at the $L/D = 40$ value.

REFERENCES

1. Schmidt, E.; Eckert, E.; and Grigull, U.: Heat Transfer by Liquids Near the Critical State. Trans. No. F-TS-527-RE, AAF, Air Material Command, Apr. 26, 1946.
2. Dickinson, N. L.; and Welch, C. P.: Heat Transfer to Supercritical Water. Paper 57-HT-7, ASME, Aug. 1957.
3. Powell, Walter B.: Heat Transfer to Fluids in the Region of Critical Temperature. Jet Propulsion, vol. 27, no. 7, July 1957, pp. 776-783.
4. Bringer, R. P.; and Smith, J. M.: Heat Transfer in the Critical Region. AIChE J., vol. 3, no. 1, Mar. 1957, pp. 49-55.
5. Goldmann, Kurt: Heat Transfer to Supercritical Water at 5000 Psi Flowing at High Mass Flow Rates Through Round Tubes. International Developments in Heat Transfer. ASME, 1963, pp. 561-568.
6. Petukhov, B. S.; Krasnoschekov, E. A.; and Protopopov, V. S.: An Investigation of Heat Transfer to Fluids Flowing in Pipes Under Supercritical Conditions. International Developments in Heat Transfer. ASME, 1963, pp. 569-578.
7. Hendricks, R. C.; Graham, R. W.; Hsu, Y. Y.; and Medeiros, A. A.: Correlation of Hydrogen Heat Transfer in Boiling and Supercritical Pressure States. ARS J., vol. 32, no. 2, Feb. 1962, pp. 244-252.
8. Wood, Rodney D.; and Smith, J. M.: Heat Transfer in the Critical Region - Temperature and Velocity Profiles in Turbulent Flow. AIChE J., vol. 10, no. 2, Mar. 1964, pp. 180-186.
9. Swenson, H. S.; Carver, J. R.; and Kakarala, C. R.: Heat Transfer to Supercritical Water in Smooth-Bore Tubes. J. Heat Transfer, vol. 87, no. 4, Nov. 1965, pp. 477-484.
10. Deissler, R. G.: Heat Transfer and Fluid Friction for Fully Developed Turbulent Flow of Air and Supercritical Water with Variable Fluid Properties. Trans. ASME, vol. 76, no. 1, Jan. 1954, pp. 73-85.
11. Hsu, Yih-Yun; and Smith, J. M.: The Effect of Density Variation on Heat Transfer in the Critical Region. J. Heat Transfer, vol. 83, no. 2, May 1961, pp. 176-182.
12. Szetela, E. J.: Heat Transfer to Hydrogen Including Effects of Varying Fluid Properties. ARS J., vol. 32, no. 8, Aug. 1962, pp. 1289-1292.
13. Hess, H. L.; and Kunz, H. R.: A Study of Forced Convection Heat Transfer to Supercritical Hydrogen. J. Heat Transfer, vol. 87, no. 1, Feb. 1965, pp. 41-48.

14. Wiederecht, D. A. ; and Sonnemann, G. : Investigation of Nonisothermal Friction Factor in the Turbulent Flow of Liquids. Paper 60-WA-82, ASME, 1960.
15. Griffith, J. D. ; and Sabersky, R. H. : Convection in a Fluid at Supercritical Pressures. ARS J., vol. 30, no. 3, Mar. 1960, pp. 289-291.
16. Graham, Robert W. ; Hendricks, Robert C. ; and Ehlers, Robert C. : Analytical and Experimental Study of Pool Heating of Liquid Hydrogen Over a Range of Accelerations. NASA TN D-1883, 1965.
17. Knapp, Karl K. ; and Sabersky, Rolf H. : Free Convection Heat Transfer to Carbon Dioxide Near the Critical Point. Int. J. Heat Mass Transfer, vol. 9, no. 1, Jan. 1966, pp. 41-51.
18. Hall, W. B. ; Jackson, J. D. ; and Khan, S. A. : An Investigation of Forced Convection Heat Transfer to Supercritical Pressures. Third International Heat Transfer Conference. Vol. 1. AIChE, 1966, p. 257.
19. Hanratty, Thomas J. : Turbulent Exchange of Mass and Momentum With a Boundary. AIChE J., vol. 2, no. 3, Sept. 1956, pp. 359-362.
20. Einstein, H. A. ; and Li, Huon: The Viscous Sublayer Along a Smooth Boundary. Proc. ASCE, vol. 82, no. EM2, Apr. 1956.
21. Runstadler, Peter W. : An Experimental Investigation of the Flow Structure of the Turbulent Boundary Layer. Ph.D. Thesis, Stanford University, 1963.
22. Bakewell, Henry P., Jr. : An Experimental Investigation of the Viscous Sublayer in Turbulent Pipe Flow. Pennsylvania State Univ., Sept. 1966. (Available from DDC as AD-639804.)
23. Mitchell, James E. ; and Hanratty, Thomas J. : A Study of Turbulence at a Wall Using an Electrochemical Wall Shear-Stress Meter. J. Fluid Mech., vol. 26, pt. 1, Sept. 1966, pp. 199-221.
24. Sternberg, Joseph: A Theory for the Viscous Sublayer of a Turbulent Flow. J. Fluid Mech., vol. 13, pt. 2, June 1962, pp. 241-271.
25. Hendricks, Robert C. ; Graham, Robert W. ; Hsu, Yih Y. ; and Friedman, Robert: Experimental Heat-Transfer Results for Cryogenic Hydrogen Flowing in Tubes at Subcritical and Supercritical Pressures to 800 Pounds Per Square Inch Absolute. NASA TN D-3095, 1966.
26. Hendricks, R. C. ; Simoneau, R. J. ; and Friedman, R. : Heat-Transfer Characteristics of Cryogenic Hydrogen From 1000 to 2500 Psia Flowing Upward in Uniformly Heated Straight Tubes. NASA TN D-2977, 1965.

27. Miller, W. S.; Seader, J. D.; and Trebes, D. M.: Supercritical Pressure Liquid Hydrogen Heat Transfer Data Compilation. Rep. R-6129, Rocketdyne Div., North American Aviation, Apr. 1965.
28. Hsu, Yih-Yun; Cowgill, Glenn R.; and Hendricks, Robert C.: Mist-Flow Heat Transfer Using Single-Phase Variable-Property Approach. NASA TN D-4149, 1967.
29. Graham, Robert W.; and Hendricks, Robert C.: Assessment of Convection, Conduction, and Evaporation in Nucleate Boiling. NASA TN D-3943, 1967.
30. Mickley, H. S.; and Fairbanks, D. F.: Mechanism of Heat Transfer to Fluidized Beds. *AIChE J.*, vol. 1, no. 3, Sept. 1955, pp. 374-384.
31. Pigford, Robert L.; and Baron, Thomas: Hydrodynamic Stability of a Fluidized Bed. *Ind. Eng. Chem. Fundamentals*, vol. 4, no. 1, Feb. 1965, pp. 81-87.
32. Ruckenstein, E.: On Turbulent Heat or Mass Transfer. *Chem. Eng. Sci.*, vol. 21, Feb. 1966, pp. 113-116.
33. Gordier, Robert L.: Studies on Fluid Jets Discharging Normally Into Moving Liquids. Tech. Paper 28, ser. B, Univ. Minnesota, Aug. 1959.
34. Torikai, Kinichi; and Yamazaki, Toshi: The Contact Area of Boiling Bubbles on the Heating Surface. *JSME Bull.*, vol. 8, no. 32, Dec. 1965, pp. 660-669.
35. Moffat, R. J.; and Kays, W. M.: The Turbulent Boundary Layer on a Porous Plate Experimental Heat Transfer With Uniform Blowing and Suction. Rep. HMT-1, Stanford University, Aug. 1967.

1. Report No. NASA TN D-5522	2. Government Accession No.	3. Recipient's Catalog No.	
4. Title and Subtitle PENETRATION MODEL EXPLANATION FOR TURBULENT FORCED-CONVECTION HEAT TRANSFER OBSERVED IN NEAR-CRITICAL FLUIDS		5. Report Date October 1969	
		6. Performing Organization Code	
7. Author(s) Robert W. Graham		8. Performing Organization Report No. E-4858	
9. Performing Organization Name and Address Lewis Research Center National Aeronautics and Space Administration Cleveland, Ohio 44135		10. Work Unit No. 129-01	
		11. Contract or Grant No.	
12. Sponsoring Agency Name and Address National Aeronautics and Space Administration Washington, D. C. 20546		13. Type of Report and Period Covered Technical Note	
		14. Sponsoring Agency Code	
15. Supplementary Notes			
16. Abstract <p>The traditional steady-state model of turbulent convection in a thermal boundary layer has been modified to include a nonsteady penetration component of heat transfer. The penetration mechanism is assumed to result from appreciable changes in the specific volume of local agglomerates of fluid near the wall under heating conditions. In some respects the penetration mechanism is similar to boiling. The overall model has been applied to forced convection of several fluids near their critical thermodynamic state. Some success has been achieved in using the model to account for the differences between the experimental data and conventional turbulent flow heat-transfer correlations for variable property fluids.</p>			
17. Key Words (Suggested by Author(s)) Near-critical fluids Penetration renewal Turbulent heat transfer		18. Distribution Statement Unclassified - unlimited	
19. Security Classif. (of this report) Unclassified	20. Security Classif. (of this page) Unclassified	21. No. of Pages 31	22. Price* \$3.00

*For sale by the Clearinghouse for Federal Scientific and Technical Information
Springfield, Virginia 22151